23 Engineering Glassy Chalcogenide Materials for Integrated Optics Applications

Kathleen Richardson, Thierry Cardinal, Martin Richardson, Alfons Schulte, and Sudipta Seal

23.1 Introduction

Next generation devices for telecommunication and related applications will rely on the development of materials which possess optimized physical properties that are compatible with packaging requirements for systems in planar or fiber form. This allows suitable "integration" to existing fiber-based applications and hence requires appropriate consideration to material choice, its stability and long-term aging behavior. Included within this chapter are results of recent efforts to engineer materials suitable for such integration. First, needs for integrated optics and the attractiveness of chalcogenide-based glasses (ChGs) are reviewed. Second, the flexibility offered within the As–S–Se glass system is discussed, and comparisons are drawn between glasses in bulk and film forms. Following a description of the chemical systems and the properties evaluated on materials in bulk glass and film form, results of efforts to create components and characterize key structural attributes of such elements are described. The property differences and characterization tools employed to realize these data are presented. Efforts have been made in these studies to process and characterize the resulting structures in the form to be used in their final device geometry. Lastly, the ability to photo-induce changes within these glasses are discussed and key issues of such modification are reviewed. Described are results of efforts to tailor optical properties concurrent with structural stability, and to evaluate changes to these properties which result during photo-modification and subsequent aging.

23.2 Chalcogenide Glasses for Near-Infrared (NIR) Optics

Two characteristics of As–S–(Se) compounds – a large glass forming region and a wide optical transmission band, with potentially low loss for the 1.3–1.55 μm telecommunications window – make them excellent candidates for infrared guiding applications. The ability to process these glasses in substantial quantities in their bulk form, and their demonstrated capability of fabricating good optical quality thin films formed by thermal evaporation and other deposition techniques, enables the realization of relatively low cost As–S–(Se) integrated optical components. With appropriate consideration of function and application, such components can be "integrated" onto a single "chip" or substrate.

In complementary work to that described elsewhere in this text, we and our collaborators have demonstrated a range of optical functions that can be realized in these glasses, including rare earth (Pr and Er) doping and emission in key telecommunication wavelengths, fabrication

Photo-Induced Metastability in Amorphous Semiconductors. Edited by Alexander V. Kolobov

ISBN: 3-527-40370-1

of waveguides (channel, self-written, fs-written), that can laterally or vertically couple light to various locations within a planar structure, and gratings (relief and phase) that can spectrally filter or modulate light. The results, summarized below, illustrate the attractiveness of these materials for such applications.

ChGs are photosensitive when exposed to bandgap energy ($E_g \sim 2.35$ eV for As_2S_3) [1,2]. Taking advantage of these photosensitive effects (photodarkening and photoexpansion) in ChGs, allows the creation of bulk waveguide structures [3], or the patterning of photo-induced relief gratings and guided wave structures in ChG films [4–6]. Recent results by our group in this area are presented later in this chapter. The interplay between micro-structure and desirable properties of devices is illustrated in materials suitable for use in high-speed optical communication applications. Such applications require all-optical processing and switching capabilities which must be compatible with system configurations, possess ultrafast broadband response time, as well as low linear and nonlinear loss. Additionally, the material must be amenable to the small sizes and stability requirements needed for future "on chip" devices. Chalcogenide glasses (ChGs) have shown promise in that they exhibit properties compatible with the above requirements at 1.3 and 1.55 μm wavelengths [7]. Recent experiments on As–S, As–S–Se and related compounds have demonstrated flexibility in forming fiber and film devices such as narrow-band spectral Bragg filters [8] and lens-arrays, rare earth doped structures [9,10] as well as couplers and self-written planar waveguides made from single and multilayer film structures [11].

Key to the realization of components in any optical communication system, is a knowledge that the material can carry out its function and maintain stability over specified thermal, mechanical and environmental conditions, for a defined lifetime. Hence, the most attractive material is only useful if a full understanding of its performance can be made in its "use" geometry. Thus, results of our studies to engineer chalcogenide glasses for optical applications have focused on the key property performance of the glasses in the final device geometry. We have sought to define fundamental differences associated with processing and use, to identify long-term stability issues and resolve them, with compositional and processing modifications.

23.3 Bulk Chalcogenide Glasses (ChG): Composition and Optical Properties

Two kinds of glass samples have been used throughout the results reported here: binary stoichiometric arsenic trisulfide (As_2S_3 or $As_{40}S_{60}$) or its selenide analogue, originating from a commercial source or prepared by a distillation process. The commercial samples, depending on the lot, exhibited regions with dark particles observed by optical microscopy. These dark particles were identified as carbon particles by Fourier transform infrared (FTIR) spectroscopy, through measurement of an optical vibration mode at 1500 cm^{-1} characterizing the C–S bonds. In order to improve the optical quality of glasses by removing potentially absorptive inclusions, a distillation procedure was established. The second type of samples were ternary As–S–Se glasses containing $\leq$40 mol% As. The fabrication procedure employed to obtain inclusion-free bulk glass material is described in detail in [12].

Table 23.1: Compositions, density ρ, glass transition temperature T_g, and energy gap E_g of bulk binary and ternary glasses.

Glass number	Composition	ρ (g/cm^3) ($\pm$ 0.01)	T_g (°C) ($\pm$ 2°C)	E_g (eV)
1	$As_2S_3(As_{40}S_{60})$	3.20	215	2.13
2	$As_{40}S_{45}Se_{15}$	3.56	207	1.88
3	$As_{40}S_{30}Se_{30}$	3.92	202	1.72
4	$As_{40}S_{15}Se_{45}$	4.27	196	1.62
5	$As_{40}Se_{60}$	4.59	191	1.54
6	$As_{32}S_{34}Se_{34}$	3.74	154	1.75
7	$As_{24}S_{38}Se_{38}$	3.63	131	1.74
8	$As_{18}S_{41}Se_{41}$	3.50	114	1.72
9	$As_{24}S_{76}$	2.67	147	2.06
10	$As_{24}S_{57}Se_{19}$	3.11	137	1.72
11	$As_{24}S_{19}Se_{57}$	4.05	122	1.51
12	$As_{24}Se_{76}$	4.46	116	–
13	$As_{14}S_{43}Se_{43}$	3.43	100	1.70

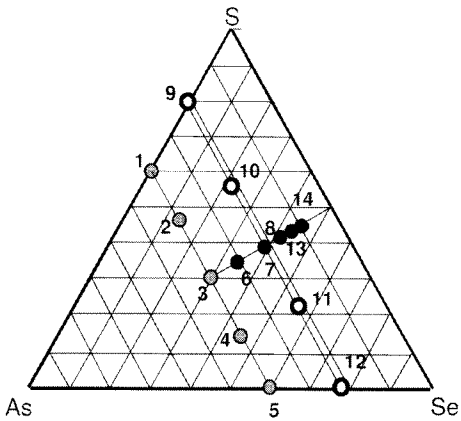

Figure 23.1: Ternary phase diagram depicting the three series of glasses examined within the As–S–Se system.

The bulk glass compositions examined for variation of optical properties with structure [13] are illustrated in the ternary phase diagram shown in Fig. 23.1. The physical properties are summarized in Table 23.1. Shown in Fig. 23.1 are three series of glasses; compositions along the line x $As_{40}S_{60} - (1 - x)$ $As_{40}Se_{60}$ form glasses where the molar ratio As/(S + Se) was held constant at 2:3, and a systematic replacement of sulfur by selenium was made. These compositions are represented as shaded circles and are labeled as compositions 1–5. Compositions maintaining a molar ratio S/Se = 1 were examined as a function of molar ratio As/(S + Se). These compositions are represented in Fig. 23.1 as solid circles and represent a systematic

reduction in $As(S,Se)_{3/2}$ pyramidal units and a concurrent increase in chalcogen-containing interconnecting chain members. To evaluate the role of chalcogen type and concentration on both structure and linear and nonlinear optical properties, a series of compositions, (numbered 8–12) were included. All glasses in this series contained 24 mol% As with an (S + Se) content equal to 76 mol%, and are shown as heavy-lined open circles.

As can be seen in Table 23.1, there is a systematic red shift of the bandgap, E_g, which is correlated with the progressive substitution of selenium for sulfur in the glass. Concurrently, an increase in density and decrease in T_g for increasing Se content occur. In the As–S and As–Se systems, a decrease of the As(S,Se) ratio produces a blue shift of the band gap [14]. For glasses with Se/S = 1, the bandgap shows much less of a change. It is important to consider the point where the two-photon absorption (2PA) of a candidate glass becomes significant. For use at the telecommunication wavelength of 1.55 μm, this point ($h\nu/2$) is near 2.0 eV. Hence glasses with a bandgap near or below this level may have appreciable nonlinear absorption that could compromise performance in high power applications.

In Fig. 23.2, several characteristic Raman excitation wavelengths are illustrated with respect to a plot of the glasses' absorption coefficients for compositions with constant As/(S + Se) molar ratio. As will be discussed later, the selection of a probe wavelength for Raman structural studies within this system becomes important, as excitation at wavelengths within or close to the bandgap may promote absorption. The magnitude of this absorption in most cases (observed for power levels as low as hundreds of microwatts) is sufficient to impart measurable photo-induced structural changes. Often, such changes result in a discoloration, or the well-referenced phenomenon of photodarkening. As will be described within this work, all Raman-based structural studies have utilized low-power (< 25 mW), near-infrared ($\lambda = 840$ nm) excitation, unless stated otherwise.

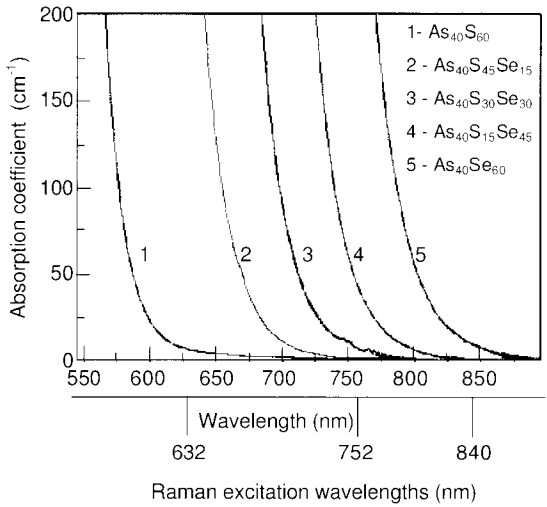

Figure 23.2: Absorption coefficient (cm $^{-1}$) versus wavelength for $As_{40}(S + Se)_{60}$ glasses illustrating the red shift in the absorption band with Se addition (from [7]). Shown for comparison are the glass band edge as compared with Raman excitation wavelengths.

The linear optical properties within the As–S–Se glass system exhibit predictable systematic variation. Like the bandgap variation with Se addition depicted in Fig. 23.2, the same glasses show a monotonic increase in linear index, n, with Se addition, when measured at 1.55 μm. This change in index for the same twelve glasses depicted in Fig. 23.1 is shown in Fig. 23.3a. The change of index with composition can be directly related to the variation in glass network structure associated with the compositional variation. The effect of an increase in 2-coordinated chalcogen (S or Se) at the expense of 3-coordinated As gives rise not only to a decrease in density, but also a concurrent decrease in refractive index. This is shown in Fig. 23.3b where index is plotted as a function of structural connectivity. This connectivity, is often described by a glass average coordination number (ACN), where the higher the ACN, the larger is the extent of connectivity. ACN within the glass system has been calculated using the following equation:

$$\text{ACN} = 3x + 2y$$

where x and y are the respective molar fractions of As and chalcogen species, respectively, and the integer represents the normal coordination state of the atom in the glass network. The systematic substitution of Se for S does not change the ACN as shown in Fig. 23.3b (as x and * for stoichiometric (40 mol%) and As-deficient (24 mol% As) compositions, respectively). However, for equi-molar chalcogen glasses (shown as triangles) the impact of decreasing content of 3-coordinated (As) species on the glass network and refractive index is clearly seen in the systematic decrease in n.

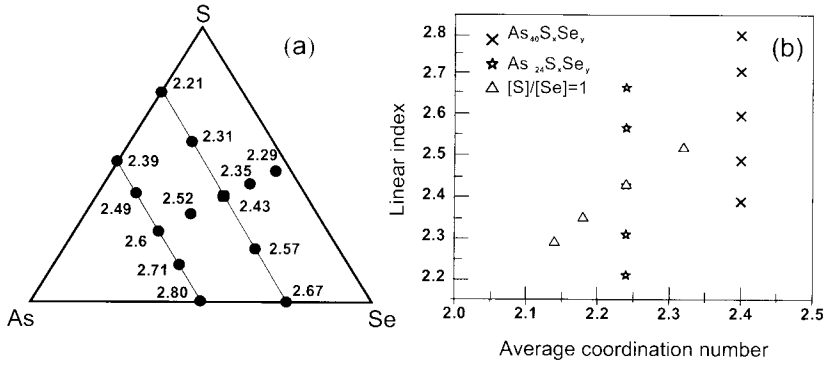

Figure 23.3: Variation in linear refractive index (n) measured at 1.55 μm as determined from Fresnel loss measurements (a) for the three series examined within the As–S–Se system ($n \pm 0.007$), and (b) the corresponding relationship between index and average coordination number (ACN) of the glass network (from [31]).

The structural changes which impact linear index variation shown in Fig. 23.3 also lead to a variation in the glass nonlinear refractive index. Here, not only are the structural species important but their electronic character also plays a role. We have carried out extensive analysis on bulk and ChG film [15, 16] materials using X-ray photoelectron spectroscopy (XPS), to probe the variation in structural and electronic properties as a function of composition and following exposure to a variety of environmental conditions [17]. These studies have confirmed

a systematic variation in position of the band edge, and limited variation in properties when exposed to severely oxidizing conditions. Understanding changes in electronic structure aid in the interpretation of many optical properties.

The normalized nonlinear index n_2 as compared with fused silica for selected glasses measured using z-scan at 1.55 μm [12] is shown in Fig. 23.4a. The enhancement of nonlinear optical properties (n_2) by substitution of selenium for sulfur in $As_{40}S_{60}$ has been attributed to an increasing number of covalent, homopolar bonds. On the other hand, distinctly large nonlinear optical property values with *ordinary linear values* in $As_{21}S_{38}Se_{38}$ (composition 7 in Fig. 23.3) may be due to Se–Se bonds, created by an As deficiency. Hence, what the chemical species is, and what its electronic structure is, impact both linear and nonlinear optical properties of the material.

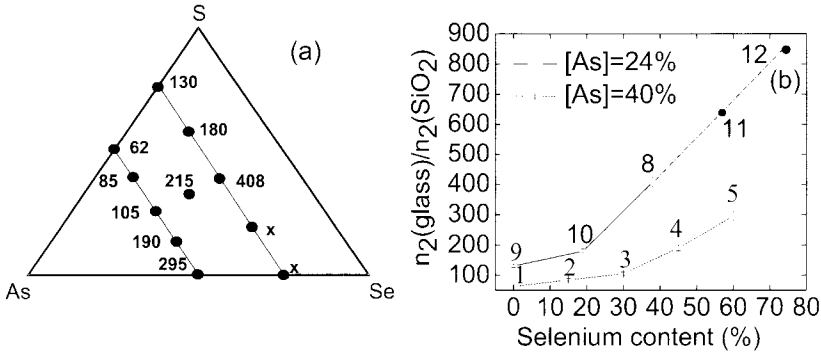

Figure 23.4: Variation in nonlinear refractive index as measured at 1.55 μm via z-scan (a) within the As–S–Se system, and (b) plotted as a function of Se content. (Extrapolated data points are preliminary data from a limited set of measurements.)

In the light of the above structural discussion, it is thought that the homopolar bonds and their electron-laden lone pairs allow strong coupling of the electric field vector of the probing laser light to the material leading to an enhanced nonlinearity. This is illustrated in Fig. 23.4b which shows the variation in measured and extrapolated values of the n_2 ratio with chalcogen content. Increasing the chalcogen content (from 60 to 76 mol%) leads to an increase in the n_2 ratio to silica and we believe the pronounced rise is attributable to the much larger quantity of Se–Se bonds (versus S–S or S–Se) as determined by Raman spectroscopy [13]. While S–S and S–Se bonds also possess two lone pairs per atom, these pairs have lower orbital electron densities and are present in much fewer numbers as compared with more polarizable Se–Se bonds. Structural analysis of these glasses has shown that the S present in these equi-molar compositions tends to remain with the As pyramidal units, while the Se form the dominant chain species. It is repeated here however, that the enhancement to n_2 offered by increasing the concentration of the n_2-enhancing species (in this case Se) comes at a price. Increasing Se content increases the linear (and nonlinear) absorption of the glass. This means that the enhancement seen is more dominated by a now present, resonance effect (the glass absorption edge falls below the $h\nu/2$ guideline for non-resonant behavior); this means that the increased absorption realized in the material can also contribute to other deleterious effects, such as

measurement-induced structural modification. Such modification under specific conditions, could lead to changes in the material structure/properties during use. Hence, a choice needs to be made whereby the magnitude of n_2 is weighted against a deleterious concurrent increase in absorption. For switching applications, both properties need be considered in the selection of an optimal material.

23.4 Chalcogenide Thin Films and Comparison with Bulk Glass

Chalcogenide thin films have been studied extensively for their variation from the parent bulk glass material and their stability in physical properties following deposition. As properties of a glass are a function of its thermal history it is not unexpected that films or fibers may have properties that vary from those seen in their melt-derived bulk analogues. Similar measurement of fiber properties within the As–Se system [18] showed similar variation in properties with forming conditions. As–S–Se films evaluated in this study show a range of property variation from their parent bulk glasses.

All glass films examined in our studies have been processed at Laval University's Centre Optique, Photonique at Laser (COPL) facilities using a clean room fabrication facility dedicated to processing ChG materials. Processing conditions, summarized for films and subsequently fabricated gratings, are discussed in detail in [11, 19]. In all cases, films are deposited from thermally evaporated parent bulk glasses, onto room temperature, oxidized silicon substrates under a vacuum of nominally 10^{-7} Torr. Glassy films processed by these techniques were confirmed to be amorphous in nature and vary in composition from the parent bulk by less than 5 mol%. [7] Most single- or multilayer films that have been prepared are approximately 2 μm in thickness or less [20]. Shown in Fig. 23.5 is a scanning electron micrograph of a multilayer ChG film structure midway through its lithographic processing steps, en route to becoming a channel waveguide. To fabricate the multilayer film structure, two bulk glass compositions were loaded into the deposition chamber and alternately deposited to form a multilayer structure. A channel within the core ternary glass serves to guide.

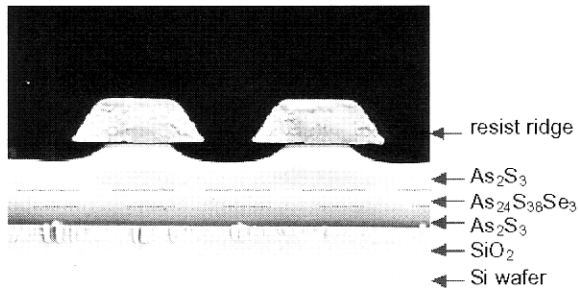

Figure 23.5: SEM micrograph of a multilayer $As_{24}S_{38}Se_{38}/As_2S_3$ ridge directional coupler midway through its lithographic processing protocol.

To compare the properties of films with those of their bulk counterparts, a series of optical and structural analyses were carried out. As described in detail by Laniel et al. [21] a systematic set of measurements were performed on films prepared under identical deposition conditions to examine the variation in film refractive index. refractive index data were collected at wavelengths surrounding the 1.55 μm telecom wavelength, and these data are summarized in Table 23.2. Shown are data for glasses numbered 1–8 from the bulk glass ternary series. Bulk glass starting compositions are shown, and unless listed (in parentheses below the parent composition), film compositions were identical with that of the parent material, as quantified through use of microprobe analysis. Values of index prior to and following a two-hour annealing at 120 °C are also tabulated.

Within the error of the measurements, no apparent variation in index was measured via the grating coupling technique over the 1.53–1.60 μm spectral range of the measurements. As compared with changes in bulk glass refractive indices with composition shown in Fig. 23.3a, film indices exhibited slightly larger variation with composition. This variation may be attributable to subtle compositional variations and the higher cooling rate with which the film structure assembles from the vapor phase. The ability for molecular species to assemble in the vapor phase [22] would give rise to a notably more ordered, connected molecular structure as compared with systems where no molecular ordering is believed to occur (e.g. in ternary As–S–Se glasses). Annealing of the as-deposited films resulted in a further increase in index and density, as the frozen network structure relaxes and further polymerizes. As illustrated in the subsequent section, these structural changes can be readily identified with Raman spectroscopy. Films exhibited an almost 2% higher linear index as compared with bulk glasses, and annealing increased the film density (decreased the as-deposited film volume) and index by a further 2%.

Densification and thickness changes have been reported in other studies within our group for fresh, annealed and aged films, as examined using Rutherford backscattering spectroscopy (RBS) [23,24]. Structural relaxation and subsequent rearrangement occur in both the short and long timeframes and dictate the aging kinetics of the materials. These changes are quantified in subsequent sections as corroborated by Raman spectroscopic analysis. Such long-term property modification, if any, is important in specific device structures.

23.5 Structural Characterization of Chalcogenide Glasses

23.5.1 Raman Spectroscopy

Inelastic scattering of light – or Raman scattering – in a material yields structural and dynamic information on a molecular level. The Raman spectrum provides a "fingerprint" of the molecular species present. The non-destructive nature of the probe, flexibility in sampling arrangements, and a technical revolution [25,26] in multichannel detection and prefilters have opened up many new areas where Raman measurements have proven valuable [27,28].

As discussed earlier, efforts to optimize film properties and device performance have focused on identifying the chemical and structural origin of the linear and nonlinear response in terms of the material processing conditions used in creating the optical element [13]. Important to this study, NIR Raman spectroscopy affords new opportunities in the non-destructive

Table 23.2: refractive index and dispersion data for chalcogenide films: as-deposited (n-a) and following annealing (a). Composition data shown are from electron microprobe analyses of resulting film. Compositional variation from the parent bulk (starting composition shown in italics) is noted where film stoichiometry showed differences.

Glass Number	Composition		Refractive index at 1.53 μm	Error	Refractive index at 1.55 μm	Error	Refractive index at 1.575 μm	Error	Refractive index at 1.60 μm	Error
1	$As_{40}S_{60}$	a	2.4035	0.0086	2.4050	0.0061	2.3964	0.0102	2.4012	0.0066
		n-a	2.3439	0.0044	2.3439	0.0037	2.3439	0.0060	2.3427	0.0030
2	$As_{36}S_{49}Se_{15}$	a	2.4707	0.0064	2.4636	0.0023	2.4618	0.0023	2.4655	0.0020
	($As_{40}S_{45}Se_{15}$)	n-a	2.4139	0.0020	2.4098	0.0020	2.4118	0.0020	2.4155	0.0020
3	$As_{39}S_{29}Se_{32}$	a	2.5727	0.0030	2.5709	0.0062	2.5714	0.0030	2.5686	0.0081
	($As_{40}S_{30}Se_{30}$)	n-a	2.5074	0.0035	2.4949	0.0024	2.5000	0.0026	2.4972	0.0041
4	$As_{10}S_{14}Se_{16}$	a	2.6750	0.0052	2.6766	0.0084	2.6766	0.0178	2.6655	0.0051
	($As_{10}S_{15}Se_{15}$)	n-a	2.6239	0.0063	2.6270	0.0063	2.6286	0.0063	2.6350	0.0064
5	$As_{40}Se_{60}$	a	2.8318	0.0059	2.8318	0.0077	2.8257	0.0030	2.8282	0.0030
		n-a	2.7842	0.0144	2.7707	0.0040	2.7715	0.0040	2.7835	0.0100
6	$As_{32}S_{34}Se_{34}$	a	2.5400	0.0028	2.5414	0.0028	2.5455	0.0069	2.5527	0.0051
		n-a	2.5050	0.0024	2.5041	0.0026	2.5064	0.0041	2.5223	0.0041
7	$As_{24}S_{38}Se_{38}$	a	2.4666	0.0023	2.4650	0.0023	2.4666	0.0042	2.4666	0.0031
		n-a	2.4445	0.0029	2.4445	0.0089	2.4445	0.0043	2.4464	0.0029
8	$As_{18}S_{11}Se_{11}$	a	2.3764	0.0020	2.3745	0.0020	2.3745	0.0020	2.3745	0.0020
		n-a	2.3691	0.0023	2.3673	0.0023	2.3709	0.0037	2.3691	0.0037

analysis of materials, which are strongly absorbing in the visible. A distinct advantage over the more conventional approach using the visible range of the spectrum is the ability to obtain the Raman spectrum of photosensitive compounds without interference from photoreactions caused by the probe beam. In chalcogenide glasses shifting the excitation wavelength to 840 nm (below the bandgap) allows one to obtain high-quality Raman spectra without material modification. The higher spatial resolution necessary to characterize planar films can be achieved with a microscope attachment.

In the microstructural analysis of single- and multilayer waveguide devices, Raman spectroscopy employing integrated optical techniques can be extremely powerful [66]. The material of interest is cast into a slab waveguide, thereby significantly increasing both the scattering volume and the electrical field intensity within the film. In spite of its sensitivity, waveguide Raman spectroscopy (WRS) using guided mode excitation [29,30] has not been applied to the structural characterization of chalcogenide glasses until recently [31,32]. Discussed here are selective results of such experiments where chalcogenide film Raman spectra were measured using guided mode excitation.

Raman scattering in the NIR is excited with 840 nm radiation from a tunable Ti:sapphire laser (30–50 mW), as depicted in Fig. 23.6. The scattered Raman light is analyzed with a single-grating spectrograph equipped with a thinned, back-illuminated CCD detector. The Rayleigh line is suppressed with a semiconductor bandgap filter [33]. The spectra shown in the following were not corrected for the instrument profile, nor was any smoothing or background correction performed.

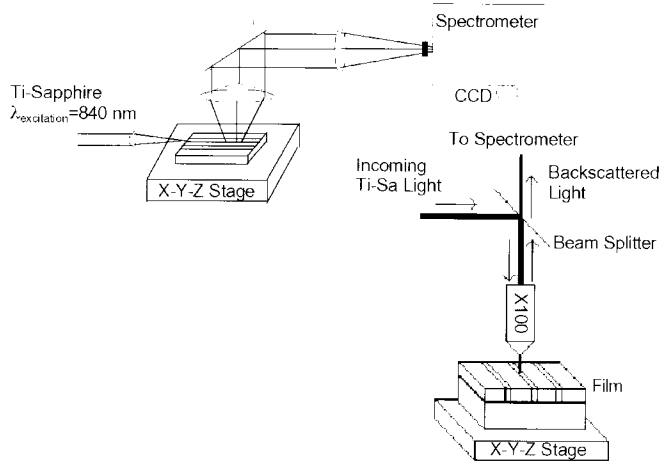

Figure 23.6: Experimental setup for near-infrared Raman spectroscopy. Sampling arrangements for micro- (backscattered geometry) and waveguide excitation (90° geometry) are shown.

23.5.2 NIR Raman Spectroscopy of Bulk Chalcogenide Glasses

Figure 23.7 illustrates the near-infrared Raman spectra (incident and scattered polarization resolved along the z-axis) for a series of binary and ternary ChG compounds. The spectra

were obtained at a spectral resolution of 1.5 cm^{-1} which is verified by resolving the isotope splitting of the symmetric stretch vibration of Cl in CCl_4 near 459 cm^{-1}.

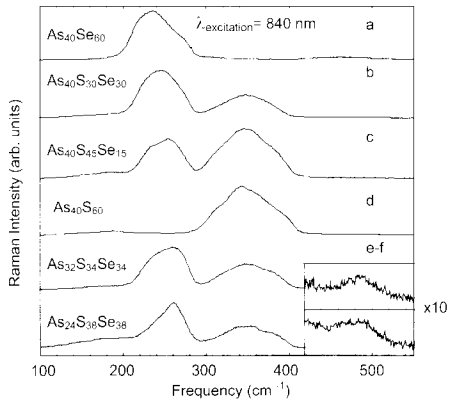

Figure 23.7: Raman spectra of bulk glasses obtained with near-infrared excitation (λ = 840 nm) as a function of compositional variation. Spectral resolution is 1.5 cm^{-1}.

The increased spectral resolution of the bulk spectra clearly shows that each of the dominant bands consist of several overlapping components. The dominant feature in the binary sulfide and selenide compounds are bands at 345 cm^{-1} ($As_{40}S_{60}$) and 230 cm^{-1} ($As_{40}Se_{60}$), respectively. These spectra are in good agreement with previous studies [34], and the strong, broad band is attributed to an anti-symmetric As–(S,Se)–As stretching vibration in the $As(S,Se)_3$ pyramids. According to the analysis of Lucovsky and Martin [35], the normal modes of the bulk glasses (e.g. clusters of $As(S,Se)_3$) molecules with weak intermolecular coupling) are obtained by treating the molecular pyramid modes ($As(S,Se)_3$) and bridging chain modes (As–(S,Se)–As) independently. In the ternary compounds with S/Se = 1 molar ratio and decreasing As content, a progressive decrease of these broad bands is observed, indicative of a decrease in the number of As-containing pyramidal sites. New bands appearing around 255 cm^{-1} and 440–480 cm^{-1} form in the now chalcogen-rich glasses, and are attributed to Se–Se and S–S homopolar bonds. These units serve as chalcogen chains connecting the remaining pyramidal units. The small number of S–S bonds indicated by a weak band near 495 cm^{-1} for equal concentrations of S and Se suggests that the S stays with the remaining pyramids, and that it is the Se which dominates the connecting chain units. Local structural investigations using Raman spectroscopy have been carried out on As–S–Se glasses previously [34] but compared with bulk glasses, only limited comparison of the structural differences attributable to different molecular entities created during film or fiber processing have been directly made [22].

Deviations from bulk glass properties in oxide fibers have been well studied and clearly illustrate the processing-induced structural property modifications possible in highly coordinated oxide glasses [36, 37]. The extent of such compositional variation, and the resulting structural units formed, varies with the specific fiber or film processing technique used, and can be extreme or subtle depending on such variables as deposition rate, substrate temperature, deposition, draw environment (vapor chemistry) or draw rate. One might expect, as has

been observed in As_2Se_3 film and fiber materials [21], that this deviation from bulk would be larger for As–S materials than that observed in oxide glasses. Neutron scattering and X-ray diffraction studies on bulk sulfide and selenide glasses and glasses deposited as thin films [22] have shown variations in structural units on the intermediate range order scale. Depending on processing conditions, polymeric cages (based on As_4S_4 units) or less connected groups of As–S pyramidal units, were observed. More importantly, since they are different from the traditional units formed in the "bulk", they are much more *metastable*, and can be structurally modified or eliminated with post-deposition processing. Knowledge of how structural features form and how they impact physical properties including optical properties is crucial to optimize desirable film properties and stability.

23.5.3 NIR Waveguide and Micro-Raman Spectroscopy of Chalcogenide Films

Waveguide Raman spectroscopy (WRS), using guided mode excitation [29, 30] has been applied to thin organic and polymeric films, to probe spontaneous [38] and coherent [39] scattering, and very recently, to sol–gel derived planar germanosilicate [40] waveguides and lead titanate [41] films. The refractive index of these organic and oxide materials allows the use of high-index glass prisms such as LaSF5 ($n \sim 1.8$) for coupling a range of propagation vectors into the waveguide structure. In spite of its sensitivity, WRS has not been applied to the structural characterization of chalcogenide glasses until recently [31, 32] most likely owing to their high index ($\sim$2.45) and lack of suitable prism couplers and difficulties associated with working in the near-infrared.

Figure 23.8 illustrates the variation in Raman spectra obtained in an As_2S_3 channel (film) waveguide structure, as probed across the waveguide endface. In the cases shown, the excitation beam (840 nm) was launched into the waveguide's end-face at various lateral positions (a–d), illustrating the sensitivity of the probe to regions near the edge (c) or center (a, d) of the guide structure.

The WRS spectra obtained from bulk As_2S_3 in amorphous and crystalline form, and an as-deposited film are shown in Fig. 23.9. Though the As_2S_3film has a thickness of just 1.5 μm, the high signal-to-noise ratio achieved by guided mode excitation is evident and the low-frequency Raman peaks are well separated from interfering Rayleigh scattering.

The distinction observed between bulk spectra and that of the film structure emphasizes the resulting structural differences associated with film processing conditions. Certain key components such as the band at 345 cm^{-1} remain in all spectra. However, new substructures appear in the film spectra as compared with the broad features of the bulk spectra. These differences from bulk are due to the different (molecular) arrangements of the constituent atoms within the film. These sharp, molecular-signature structures were confirmed not to be due to crystallinity within the film, but most likely result from the formation of as-deposited As_4S_4 units [22,42]. Several sharp molecular bands superimposed on a network-like continuum have also been observed in Raman spectra excited with near band energies (647 nm) [42–44]. By using a longer excitation wavelength (840 nm) and due to the absence of changes in the spectra when varying the power (10–50 mW) we rule out photo-induced changes from the probe beam [45].

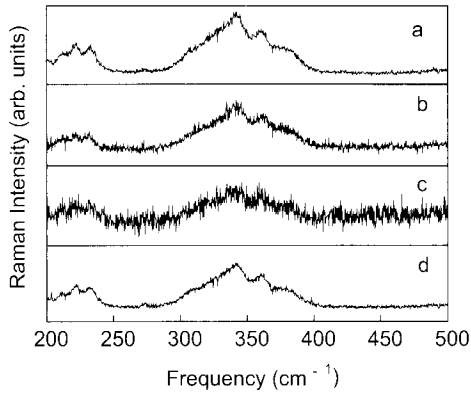

Figure 23.8: Waveguide Raman spectra of single layer, As_2S_3 channel structure. Panels (a) to (d) show a sequence traversing along the lateral direction (L to R) on the endface of the waveguide traversing from channel to channel. Excitation wavelength is 840 nm.

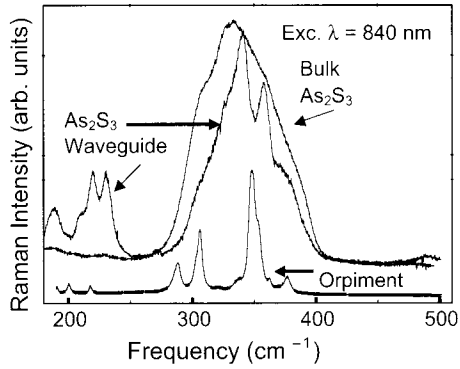

Figure 23.9: Structural features in film and bulk As_2S_3 Raman spectra as compared with high-purity crystal (from [66]). (Crystalline specimen courtesy of Prof. M. Frumar, University of Pardubice, Czech Republic).

23.6 Photo-Induced Changes in Glassy Chalcogenides

Recent publications have proposed the possibility of a refractive index change by femtosecond laser exposure of glasses in their transparent spectral region [46–48]. Most papers have reported this effect in silica or germanosilicate glasses [46]. Waveguide writing has been achieved by generating line damage inside various glasses and especially in chalcogenides [47]. Self-written waveguides have also been reported in $As_{40}S_{60}$ glass films using a femtosecond 800 nm source propagating through the films axis [48] and in bulk [7].

The photo-induced phenomenon has been widely investigated in amorphous materials. Chalcogenide glasses are well known to exhibit reversible photo-induced effects to bandgap light exposure [49–53]. The low optical bandgap of chalcogenide glasses make them highly

sensitive to visible exposure. Exposure to bandgap wavelength light induces a photodarkening in $As_{40}S_{60}$ glasses, a reduction of the glass bandgap, and a refractive index change in the exposed region according to the Kramers–Kronig relation. An important aspect of the photodarkening is that it was not observed in crystalline materials but only in disordered materials, leading to the conclusion that photodarkening effects are related to the increase of randomness of the glass network [54].

A correlation between reversible photo-induced effects and structural change has been discussed by different authors [13, 53, 55, 56] for bulk and well-annealed thin film materials. The increase of homopolar As–As and S–S chemical bonds, and of the disorder of the glass network was considered to contribute to the photodarkening effect. However, the relation between structure and photodarkening is not well established.

Discussed in this section are results of studies evaluating the effects of writing over a range of exposure conditions on ChG materials in bulk and film form. In addition to writing waveguides, we are interested in understanding the thresholds whereby laser interaction with the ChG material transitions from reversible to irreversible photostructural change, and onto permanent damage resulting from ablation.

23.6.1 Exposure Sensitivity of Chalcogenide Glasses

Photo-induced changes to a material can occur over a range of exposure conditions and in ChG materials are a function of material photosensitivity. In early work by our collaborators, [11] the photosensitivity of As_2S_3 was compared with the highly nonlinear $As_{24}S_{38}Se_{38}$ composition used in multilayer waveguide structures. It was shown that under identical exposure conditions, the ternary material exhibited dramatically reduced induced index changes following illumination with a continuous wave (CW) 514.5 nm source.

The extent of changes (both structural and optical) have been shown to vary widely with wavelength of the irradiating light (with respect to the bandgap), intensity (ns versus ps or fs pulses as compared with CW), and cumulative exposure dose. The resulting material modification associated with these conditions, range from the well-documented (reversible or irreversible) photodarkening, to irreversible destructive modification to the glass bonds during laser ablation. We are investigating the variation in structural changes imposed on bulk and film ChG materials associated with these widely differing exposure regimes, in an attempt to maximize the means by which the glasses can be modified for a range on on-chip components.

The mechanism of fs interaction in materials remains a topic of extensive research. It has been studied in detail at the University of Central Florida (UCF) with the aim of micromachining bulk materials in ambient atmosphere [53, 57]. Efforts to utilize these sources in the fundamental regimes of modification possible in ChG materials are briefly described in [57, 58], along with the fundamental mechanisms believed to be dominant in the drilling of deep holes in a range of oxide and non-oxide glass materials.

Of recent interest is the ability to generate a broad range of material response using fs laser pulses. In an effort to quantify the variation in ChG material response, we systematically increased the power density on an As_2S_3 film, evaluated the photoexpansion and ablation, and discerned where the cross-over in material behavior occurred. These results, discussed in [59], are depicted in Fig. 23.10. Shown in Fig. 23.10a are the resulting spots illuminated with sub-100 fs pulses, with power density of the exposure, shown on the x-axis. Fig. 23.10b illustrates

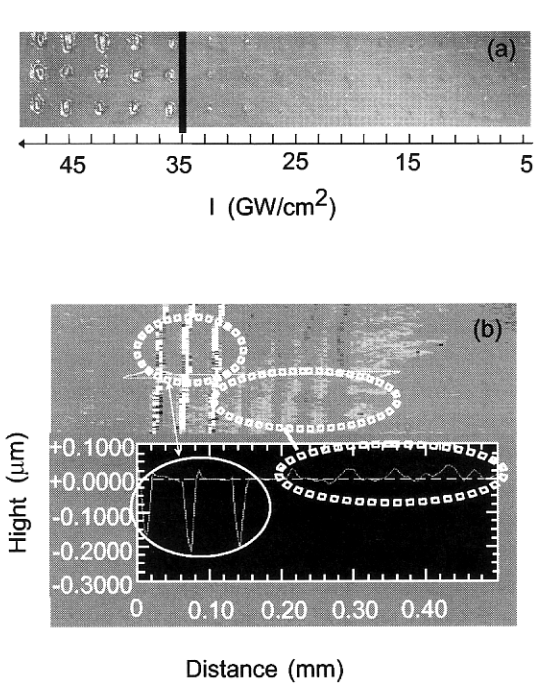

Figure 23.10: (a) Array of features written in an As_2S_3 film using fs pulses of a Ti:sapphire (λ = 800 nm) laser illustrating the power density threshold (in GW/cm^2) where photoexpansion (right of black line) transcends to laser ablation (left of black line). (b) White light interferogram and linescan illustrating topographic variation in lines written under the power density regimes identified in (a). The left features (top and bottom) correspond to trenches ablated during writing, whereas the faint regions of photoexpansion (right) occur in these films for power densities less than 35 GW/cm^2.

the change in film surface relief associated with transitioning into the ablation regime. Here, the photoexpansion seen with sub-threshold exposure, gives rise to ablative material removal, as seen in the New View 5000 White Light interferometer scans, at a threshold of 35 GW/cm^2. The mechanisms of material modification in these two forms of materials are markedly different.

23.6.2 Photo-Induced Waveguides in Bulk ChG Materials

We have written permanent waveguides in both bulk [7] and film As_2S_3 glasses [58] using a train of 850 nm femtosecond laser pulses and have measured both the induced index variation and structural changes induced through the photo-modification. An index variation in the bulk material, correlated to photodarkening was reported and corresponds to a local increase comparable with the magnitude observed in other bulk ChG studies. Micro-Raman spectroscopy has shown the local chemical change associated with the refractive index variation. It is believed that local changes in nonlinear absorption occur during the writing process, leading to a structural change and local index modification. Correlation of these optical changes with the structural modification within the bulk glass are illustrated in Fig. 23.11.

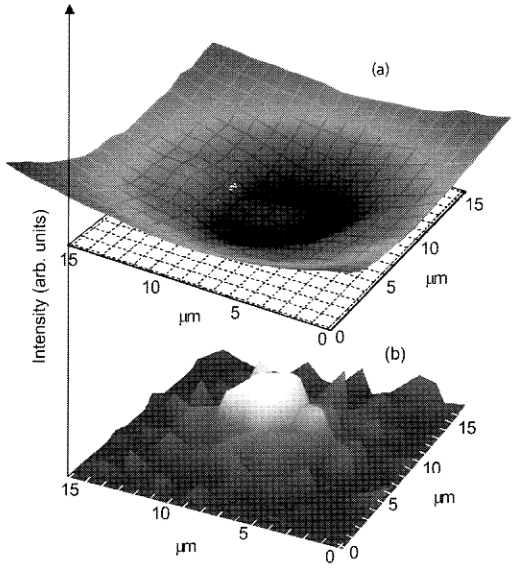

Figure 23.11: (a) Three dimensional map of Raman scattering illustrating the local evolution of the Raman bands centered at 345 cm^{-1} (a) and at 236 cm^{-1} (b) for the central region of a waveguide written in bulk As_2S_3 (from [3]). These maps correspond to the creation of homopolar As–As bonds (b) at the expense of previously existing As–S bonds (a).

The refractive index variation between the waveguide (exposed region of the glass sample) and the cladding (unexposed region) was evaluated following waveguide writing. An induced index change of $+0.04$ was associated with the formation of the 9 mm diameter circular waveguide formed by moving the sample through a well-characterized focal region. A key finding of the study defined the structural mechanism associated with the writing process in the As_2S_3 material. The concurrent destruction of As–S bonds within the glass network and the associated formation of As–As bonds during the bulk material modification is quantified by a two-dimensional micro-Raman analysis (excitation $\lambda = 752$ nm). The spatial variation of these two key bond types are shown in the plots in Fig. 23.11a and b. Figure 23.11a illustrates the local depletion of As–S bonds in the central waveguide region, as reflected in the decrease of Raman intensity of the As–S 345 cm^{-1} peak. This change is accompanied by a corresponding increase in the 236 cm^{-1} band (Fig. 23.11b) attributable to local formation of "wrong" As–As bonds. As no homopolar bonds are theoretically present in the stoichiometric bulk As_2S_3, their *formation* is characteristic of (fs) laser modification. As will be described in the next section, this mechanism is converse to the that seen during waveguide writing in films, where homopolar bonds that exist in as-deposited films actively participate in the local structural rearrangement during laser interaction.

23.6.3 Photo-Induced Changes in ChG Films

Photo-induced effects have been observed in a variety of chalcogenide glasses [41,42]. These effects include optical transmissivity and reflectivity variations, refractive index changes, and variations in chemical reactivity. Two-photon induced refractive index changes by exposure in the 800 nm region have been measured [60]. The ultimate long-term stability of chalcogenide-based optical elements relies on the generation of photo-induced structures which undergo limited structural relaxation with time. ChGs typically exhibit lower glass transition temperatures (T_g) than oxide glasses and hence can exhibit significant sub-T_g relaxation at, or near, room temperature [18]. This relaxation can result in structural changes that modify the *as-written* glass structure and performance of the optical element. To ascertain the effects of structural relaxation resulting from aging, spectroscopic analyses of As_2S_3 film structures were performed following annealing and in freshly written (<1 month) and aged (~3 years under ambient conditions) Bragg gratings. In all cases, a depletion in as-deposited/as-written As–As and S–S bonds and modification of As–S bonds, was observed. The extent of such changes depended on the initial, as-formed concentrations of each type of bond, and how the film was aged or annealed. Changes in waveguide Raman spectra for As_2S_3 structures prior to and after annealing, and following 514 nm exposure similar to that used in grating writing are shown in Fig. 23.12 and are discussed in [23, 24]. The sharp features seen in the Raman spectrum of the as-deposited film illustrated in Fig. 23.12 are not present in bulk ChGs and correspond to molecular units that can undergo reconfiguration over time.

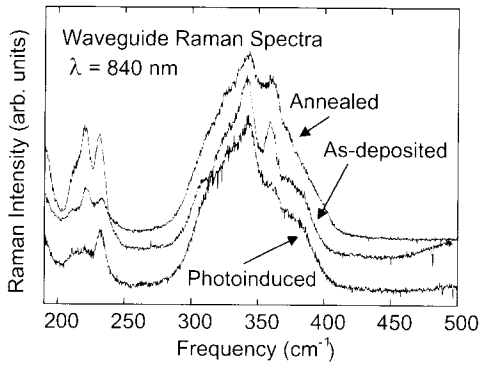

Figure 23.12: Variation in waveguide Raman spectra for fresh, annealed, and photostructurally modified As_2S_3 channel waveguide (exposure λ = 514.5 nm). Excitation wavelength is 840 nm (from [66]).

Characterization of grating structures shortly after writing, and after prolonged room temperature aging shows that while small amounts of the *as-written* relief structure stayed in the *aged* grating structure, few molecular species seen in as-deposited structures remained, and a considerable reduction in induced index change (δn) occurs.

The polarization dependence of such writing processes has been studied in ChG, most recently by our Laval colleagues in As_2S_3, and others in As–Se glasses in [61] and references therein. We are currently examining the concurrent glass structural modification in the Saliminia-written [62] structures, using micro-thermal analysis techniques [63].

The effects of photo-induced changes are evident in the Raman spectra as well. By exciting Raman scattering with sub-bandgap energies ($\lambda = 840$ nm) at low-power levels (25 mW) photostructural changes due to the probe beam are avoided. Large changes are seen in the Raman band near 235 cm^{-1} which is associated with As–As bond vibrations. Several mechanisms for photo-induced changes in chalcogenides, including bond redistribution and coordination defects, have been suggested [60]. Trigonal AsS_3 pyramidal units can be transformed into a five-fold coordinated As site having four As–S bonds and one As–As bond via a photoionization process [44]. The variation in film age and deposition technique dictates how far the film structure is from the local equilibrium state and the impact of such structural changes on expected grating optical performance. These issues are currently being examined, and recent results have shown that homopolar bonds seen in as-deposited films (shown near 200 cm^{-1} in Fig. 23.12), remain, even after aging periods of several years. Not only do these well-aged films retain their photosensitivity (i.e. undergo induced refractive index modification and structural changes (expansion)), but the magnitudes of both are comparable to that seen in freshly formed films, illuminated shortly after deposition. These results will undoubtedly lead to further progress in forming stable, written structures in these ChG materials.

23.6.4 Grating Fabrication in As_2S_3 Glassy Films

Unlike the grating fabrication techniques described above for ChG films illuminated through masks or with interfering CW beams, femtosecond (fs) lasers also appear to be a promising tool for the direct write micro-structuring of optical materials. It was demonstrated that unamplified femtosecond lasers could produce optical breakdown and structural change in bulk transparent materials using tightly focused pulses of just 5 nJ [55].

Using an extended cavity unamplified Kerr-lens mode locked Ti:sapphire laser ($\lambda = 800$ nm, repetition rate 28 MHz, sub-50 fs pulse duration, up to 20 nJ/pulse), relief and volume gratings with a 20 μm period were fabricated on a 1.66 μm thick, As_2S_3 thin film [64]. The output of the laser was focused by a 15×, 0.28 *NA* reflective objective onto a target attached to a 3D motorized translation system.

The sample was processed in two regimes: first, the intensity was kept below the ablation threshold, generating a volume grating resulting from photoexpansion and an induced index change. The resulting structure from a Zygo New View 5000 is shown in Fig. 23.13a. In the second regime, intensities *above* the ablation threshold produced a relief grating with grooves of 0.2 μm depth (Fig. 23.13b). Previous studies have linked bulk glass structural and optical property changes (photosensitivity) through Raman spectroscopy, showing that nonlinear absorption-induced index changes were linked to local bonding changes in As_2S_3 [13]. Following this approach, waveguides over 1 cm in length and ~10 μm in diameter were fabricated in As_2S_3 thin films by direct transverse writing using the same unamplified Ti:sapphire laser [67]. Further studies are under way including the measurement of the refractive index change by the refracted near-field technique. Concurrently, we are evaluating long-term stability in both photoexpansion and induced index with age, including studies on pre-aged films, which have undergone most of their short-term, post-deposition relaxation.

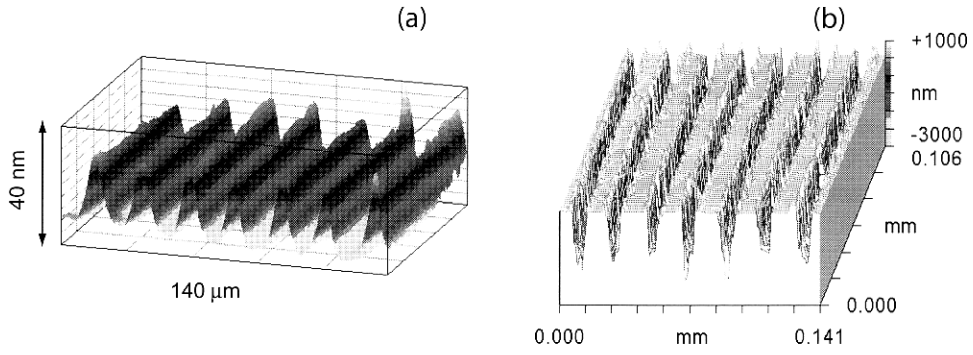

Figure 23.13: Surface profile of (a) the phase and (b) topographic relief in gratings on an As_2S_3 film produced with sub-50 fs laser pulses from the extended cavity unamplified Ti:sapphire oscillator (from [65]).

23.7 Conclusions and Outlook

This chapter has summarized a variety of results whereby ChG materials have been processed and characterized with the aim of understanding key material attributes in geometries suitable for use in integrated optical components. Within the narrow composition space where we have focused on obtaining a thorough grasp of bulk/film property trends and variation, clear learnings have been realized associated with the linear and nonlinear optical properties of these glasses and their relation to glass structure. It been shown by these efforts and those of others that compositional-tailoring of glasses to known properties can yield structures and components with good optical quality and promise of potential in-service stability. Such know-how thus allows identification of materials that can be deposited onto glass or Si chip substrates and modified to carry out key functions suitable for moving and amplifying light.

Photo-induced structural changes can be realized in ChG materials to induce structure and refractive index changes. Such modification can be used to write structures, either with CW bandgap light, or near-bandgap light employing short (fs) pulses. The photosensitivity offered by ChG materials allow polarization-dependent features to be written which may offer promising component opportunities once stabilization techniques employing pre-aging are optimized. This material flexibility, along with the technology know-how associated with true, three-dimensional structuring capabilities offered through direct write techniques, illustrate further routes to clever device engineering.

Emerging results of ongoing interest and research in ChG materials will allow a range of key components with stable optical and physical properties to be realized for next generation optical elements. Characterization of key structural features on materials in their final device configuration allows for a thorough understanding of the inter-relationship between processing and end use. Such analysis is essential in predicting long-term stability requisite for device applications.

Acknowledgments

It is a pleasure to acknowledge a host of students and collaborators who have contributed to the results discussed herein, in particular C. Rivero, A. Zoubir, G. Nootz, P. Sharek, C. Lopez, L. Shah, M. Marchivie, K. Zollinger, M. deCastro, A. Graham, W. Li, C. Wilson, K. Elshot, M. Couzi, J. Fick, D. Hagan, and R. Irwin. We are also grateful to our Canadian colleagues and their students for their long-term partnership and friendship, specifically A. Villeneuve, T. Galstian, R. Vallee, E. Knystautas, K. Turcotte, V. Hamel, K. LeFoulgoc, C. Meneghini, J. F. Viens, A. Saliminia, N. Hô, and J. Laniel. All of these participants took part in processing and characterization efforts illustrated in the results presented herein, and have contributed to this mutually rewarding collaboration. This work was carried out with the support of a number of research, equipment, and educational grants, including NSF awards DMR-9974129, DUE-9850934, INT-0129235, ECS-0123484, ECS-0225930, EEC-9732420, and CHE-9732161, and IGERT grant DGE-0114418. The authors acknowledge the assistance of staff at the AMPAC Material Characterization Facility (MCF), University of Central Florida.

References

[1] A. Villeneuve, T.V Galstian, M. Duguay, and K. Richardson, J. Light. Technol. **15**, 1343 (1997).

[2] S. Ramachandran, S. Bishop, J.P. Guo, and D.J. Brady, IEEE Phot. Tech. Lett. **8**, 1041 (1996).

[3] O.M. Efimov, L.B. Glebov, K.A. Richardson, E. Van Stryland, T. Cardinal, S.H. Park, M. Couzi, and J.L. Bruneel, J. Opt. Mater. **17**, 379 (2001).

[4] A.M. Andriesh, Y.A. Bykovskii, E.P. Kolomeiko, A.V. Makovkin, V.L. Smirnov, and A.V. Shmal'ko, Sov. J. Quantum Electron. **7**, 347 (1977).

[5] M. Asobe, T. Kanamori, and K. Kubodera, IEEE J. Quant. Electron. **29**, 2325 (1993).

[6] S. Ramachandran and S.G. Bishop, Appl. Phys. Lett. **74**, 13 (1999).

[7] K.A. Richardson, J.M. McKinley, B. Lawrence, S. Joshi, and A.Villeneuve, J. Opt. Mater. **10**, 155 (1998).

[8] K. Tanaka, N. Toyosawa, and H. Hisakuni, Opt. Lett. **20**, 1976 (1995).

[9] J. Fick, A. Villeneuve, E. Knystautas, S. Roorda, and K. Richardson, J. Non-Cryst. Solids **272**, 200 (2000).

[10] C. Meneghini, J.F.Viens, A. Villeneuve, E.J. Knystautas, M.A. Duguay, and K.A. Richardson, J. Optical Society B **15**, 1305 (1997).

[11] J.F. Viens, C. Meneghini, A. Villeneuve, T.V. Galstian, E. Knystautas, M. Duguay, K.A., Richardson, and T. Cardinal, J. Lightwave Technol. **17**, 1184 (1999).

[12] K.A. Richardson, J.M. McKinley, B. Lawrence, S. Joshi, and A. Villeneuve, J. Opt. Mater. **10**, 155 (1998).

[13] T. Cardinal, K. Richardson, H. Shim, G. Stegeman, A. Schulte, R. Beathy, K. LeFoulgoc, C. Meneghini, J.F. Viens, and A.Villeneuve, J. Non-Cryst. Solids **256 & 257**, 353 (1999).

[14] E. Hajto, P.J.S. Ewen, and A.E. Owen, J. Non-Cryst. Solids **164–166**, 901 (1993).

[15] S. Seal, K.A. Richardson, C. Lopez, A. Graham, D.K. Verma, K. Turcotte, J. Laniel, A. Saliminia, T.V. Galstian, and A. Villeneuve, Phys. Chem. Glasses **43**, 59 (2002).

[16] W. Li, S. Seal, C. Lopez, and K.A. Richardson, J. Appl. Phys. **92**, 7/02 (2002).

[17] S. Seal, W. Li, K.A. Richardson, D.K. Verma, A. Shulte, C. Lopez, A. Graham, and C. Rivero, J. Corros., in press (2002).

[18] K.A. Cerqua-Richardson, PhD Thesis, NYS College of Ceramics at Alfred University (1992).

[19] A. Saliminia, A.Villeneuve, T.V. Galstian, S. LaRochelle, and K.A. Richardson, J. Lightwave Technol. **17**, 837 (1999).

[20] C. Lopez, K.A. Richardson, S. Seal, D.K. Verma, A. Graham, A. Villeneuve, T.V. Gastian, K. Turcotte, A. Saliminia, J. Laniel, M. deCastro, A. Schulte, and C. Rivero, J. Am. Ceram. Soc. **85**, 1372 (2002).

[21] J. Laniel, J.M. Ménard, A. Villeneuve, R. Vallée, C. Lopez, and K.A. Richardson, Proc. SPIE Photonics North 2002: International Conference on Applications of Photonic Technology (ICAPT), vol. 4833, Quebec (2002).

[22] A. Apling, A.J. Leadbetter, and A. Wright, J. Non-Cryst. Solids **23**, 369 (1977).

[23] C. Rivero, P. Sharek, G. Nootz, C. Lopez, K.A. Richardson, and A. Schulte, Proc. SPIE Engineering Thin Films with Ion Beams, Nanoscale Diagnostics, and Molecular Manufacturing, vol. 4468, San Diego, CA (2001).

[24] C. Rivero, P. Sharek, G. Nootz, C. Lopez, W. Li, K. Richardson, A. Schulte, G. Braunstein, R. Irwin, V. Hamel, K. Turcotte, and E. Knystautas, Thin Solid Films, **425**, 59 (2003).

[25] R. L. McCreery, Raman Spectroscopy for Chemical Analysis, Wiley, New York, 2000.

[26] B. Chase, Appl. Spectrosc. **48**, 14A (1994).

[27] P. Colomban and J. Corset (Eds.), J. Raman Spectrosc., Special Issue: Raman (Micro) Spectrometry and Materials Science (1999).

[28] W.H. Weber and R. Merlin (Eds.), Raman Scattering in Materials Science, Springer, New York, 2000.

[29] S.L. Zhang and B.F. Zhu (Eds.), Proc. XXVIIth Intl. Conf. on Raman Spectrosc., Wiley, New York, 2000.

[30] J.F. Rabolt, in Fourier Transform Raman Spectroscopy, D. B. Chase and J. F. Rabolt (Eds.), Academic Press, San Diego, 1994, p. 133.

[31] C. Rivero, A. Schulte, C. Lopez, K. Richardson, K. Turcotte, V. Hamel, A. Villeneuve, and T. Galstian, OSA Topical Meeting on Nonlinear Guided Waves, Clearwater, FL, 2001.

[32] A. Schulte, C. Rivero, K. Richardson, K. Turcotte, J. Laniel, V. Hamel, A. Villeneuve, A. Saliminia, and T. Galstian, Opt. Commun. **198**, 125 (2001).

[33] A. Schulte, Appl. Spectrosc. **46**, 891 (1992).

[34] A. Freitas, J. Strom, and D.J. Treacy, J. Non-Cryst. Solids **59&60**, 615 (1983).

[35] G. Lucovsky and R. Martin, J. Non-Cryst. Solids **8–10**, 185 (1972).

[36] M. Goldstein and T. H. Davies, 1955, J. Am. Ceram. Soc. **38**, 223 (1955).

[37] H. Stockhorst and P. Bruckner, J. Phys. (Coll.) **43**, C9 (1982).

[38] Y. Levy, C. Imbert, J. Cipriani, S. Racine, and R. Dupeyrat, Opt. Commun. **11**, 66 (1974).

[39] W.M. Hetherington III, N.E.Van Wyck, E.W. Koenig, G.I. Stegeman, and R.M. Fortenberry, Optics Lett. **8**, 88 (1984).

[40] C. Duverger, J.M. Nedelec, M. Benatsou, M. Bouazoui, B. Capoen, M. Ferrari, and S. Turrell, J. Mol. Struct. **480–481**, 169 (1999).

[41] C. Urlacher, O. Marty, J.C. Plenet, J. Serughetti, and J. Mugnier, Thin Solid Films **349**, 63 (1999).

[42] M. Frumar, M. Vlcek, Z. Cernosek, Z. Polak, and T. Wagner, J. Non-Cryst. Solids **213&214**, 215 (1997).

[43] P. Krecmer, M. Vlcek, and S.R. Elliot, J. Non-Cryst. Solids **227–230**, 682 (1998).

[44] T. Uchino, D.C. Clary, and S.R. Elliott, Phys. Rev. Lett. **85**, 3305 (2000).

[45] A. Schulte, M. Marchivie, K. Zollinger, C. Rivero, A. Graham, C. Lopez, K.A. Richardson, K. Turcotte, and A. Villeneuve, Proc. of the XVIIth International Conference on Raman Spectrosc., (ICORS) **17**, 616 (2000).

[46] H.B. Sun, Y, Xu, S. Joudkazis, K. Sun, M. Watanabe, S. Matsuo, H. Misawa, and J. Nishii, Opt. Lett. **26**, 325 (2001).

[47] K. Hirao and K. Miura, J. Non-Cryst. Solids **239**, 91 (1998).

[48] K. Minoshima, A.M. Kowalevicz, I. Hartl, E.P. Ippen, and J.G. Fujimoto, Opt. Lett. **26**, 1516 (2001).

[49] F. Korte, S. Adams, A. Egbert, C. Fallnich, A. Ostendorf, S. Nolte, M. Will, J.P. Ruske, B.N. Chichkov, and A. Tunnermann, Opt. Express **7**, 1545 (2000).

[50] E. Matthias, M. Reichling, J. Siegel, O.W. Kading, S. Petzoldt, H. Skurk, P. Bizenberger, and E. Neske, Appl. Phys. A (Solids and Surfaces) **A58**, 129 (1994).

[51] N. Bloembergen, IEEE J. Quantum Electron. **QE-10**, 375 (1974).

[52] Schott Glass Technologies Inc., Optical Glass Catalog, 400 York Avenue, Duryea, PA 18642.

[53] L. Shah, PhD Thesis, School of Optics, University of Central Florida (2001).

[54] A. Braun, G. Korn, X. Liu, D. Du, J. Squier, and G. Mourou, Opt. Lett. **20**, 73 (1995).

[55] C.B. Schaffer, A. Brodeur, J.F. Garcia, and E. Mazur, Opt. Lett. **26**, 93 (2001).

[56] A.M. Streltsov and N.F. Borrelli, Opt. Lett. **26**, 42 (2001).

[57] L. Shah, J. Tawney, M. Richardson, and K. Richardson, Appl. Surf. Sci. **183**, 151 (2001).

[58] A. Zoubir, L. Shah, K. Richardson, and M. Richardson, Proc. SPIE, **4760-5**, 2 High Power Laser Ablation in Materials, Taos NM (2002).

[59] K.A. Richardson, A. Zoubir, C. Rivero, C. Lopez, L. Shah, and M.C. Richardson, Proc. of the XIIIth International Symposium on Non-Oxide Glasses, Parubice, Czech Republic (2002).

[60] C. Meneghini and A. Villeneuve, J. Opt. Soc. Am. B **15**, 2946 (1998).

[61] G. Chen, H. Jain, M. Vlcek, S. Khalid, J. Li, D.A. Drabold, and S.R Elliott, Appl. Phys. Lett. **82**, 706 (2003).

[62] A. Saliminia, T. Galstian, and A. Villeneuve, Phys. Rev. Lett. **85**, 4112 (2000).

[63] TA Instruments, Micro-thermal Analysis (μTA-2990) System, Delaware, 2000.

[64] A. Zoubir, M.C. Richardson, C. Rivero, C. Lopez, N. Hô., N., R. Vallée, and K.A. Richardson, Proc. Conference on Lasers and Electro-Optics, paper #CMZ4, Long Beach CA (2001).

[65] A. Saliminia, T.V. Galstian, A. Villeneuve, K. LeFoulgoc, and K.A. Richardson, J. Opt. Soc. B **17**, 1343 (2000).

[66] A. Schulte and K.A. Richardson, "Near-Infrared Raman Spectroscopy of Chalcogenide Glasses for Integrated Optics," in Recent Research Developments in Non-Crystalline Solids, Transworld Research Network, P.O. 36/248 (1) Vallakkadavu, Trivandrum - 695 008, Kerala, India (2001).

[67] C. Lopez, K. Richardson, M. Balu, D. Hagan, A. Zoubir, M.C. Richardson, J. Laniel, J.M. Menard, A.Villeneuve, and R.Vallée, OSA Annual Meeting, Orlando FL (2002).